Chin. Phys. Lett. **39**, 077501 (2022) **Express Letter**

Resistance Anomaly and Linear Magnetoresistance in Thin Flakes of Itinerant Ferromagnet Fe_3GeTe_2

Honglei Feng(冯红磊)[1,2], Yong Li(李勇)[1,2], Youguo Shi(石友国)[1,2,3], Hong-Yi Xie(解宏毅)[4], Yongqing Li(李永庆)[1,2,3], and Yang Xu(许杨)[1,2*]

[1]*Beijing National Laboratory for Condensed Matter Physics, Institute of Physics, Chinese Academy of Sciences, Beijing 100190, China*
[2]*School of Physical Sciences, University of Chinese Academy of Sciences, Beijing 100190, China*
[3]*Songshan Lake Materials Laboratory, Dongguan 523808, China*
[4]*Division of Quantum State of Matter, Beijing Academy of Quantum Information Sciences, Beijing 100193, China*

(Received 29 March 2022; accepted manuscript online 25 May 2022)

Research interests in recent years have expanded into quantum materials that display novel magnetism incorporating strong correlations, topological effects, and dimensional crossovers. Fe_3GeTe_2 represents such a two-dimensional van der Waals platform exhibiting itinerant ferromagnetism with many intriguing properties. Up to date, most electronic transport studies on Fe_3GeTe_2 have been limited to its anomalous Hall responses while the longitudinal counterpart (such as magnetoresistance) remains largely unexplored. Here, we report a few unusual transport behaviors on thin flakes of Fe_3GeTe_2. Upon cooling to the base temperature, the sample develops a resistivity upturn that shows a crossover from a marginally $-\ln T$ to a $-T^{1/2}$ dependence, followed by a lower-temperature deviation. Moreover, we observe a negative and non-saturating linear magnetoresistance when the magnetization is parallel or antiparallel to the external magnetic field. The slope of the linear magnetoresistance also shows a nonmonotonic temperature dependence. We deduce an anomalous contribution to the magnetoresistance at low temperatures with a scaling function proportional $-HT^{1/2}$, as well as a temperature-independent linear term. Possible mechanisms that could account for our observations are discussed.

DOI: 10.1088/0256-307X/39/7/077501

In recent years, the growing interest of exploring magnetic 2D van der Waals (vdW) materials has been triggered by the discovery of atomically thin magnets in the 2D limit.[1–3] They provide promising testbed for studying the interplay among magnetism, electronic structures, and correlation effects, as well as for investigating critical behaviors with reduced dimensionality.[4] The 2D nature of the thin layers also enables improved efficiency on the electrical tunability of magnetism and magnetization.[5–9] When further integrated into functional vdW heterostructures, they can be exploited for various potential spintronics applications. Among the large family of magnetic 2D vdW materials, Fe_3GeTe_2 (FGT) is one of the most important and extensively studied metallic ferromagnets. Below its Curie temperature T_c, robust ferromagnetism with strong out-of-plane anisotropy can be sustained down to the monolayer limit.[10] Large anomalous Hall effect in FGT has been observed and suggested to be induced by the Berry curvature from symmetry protected topological nodal lines [a Karplus–Luttinger (KL) mechanism], rather than the extrinsic mechanisms such as skew scattering and side jumps.[11–14] The Curie temperature T_c of the bulk crystals is about 220–230 K.[11,15,16] Few-layer FGT has been shown to exhibit tunable T_c up to 330 K (above room temperature) with the help of ionic gating.[8] The vertical spin valves with large tunneling magnetoresistance (TMR) have been recently demonstrated in FGT based junctions (such as FGT/hBN/FGT, FGT/InSe/FGT, and FGT/FGT) when the spins of the two FGT layers switch from being aligned to anti-aligned.[17–19]

However, despite many existing studies on FGT, the mechanisms regarding some of its basic properties are still unclear. For example, what gives rise to the itinerant magnetism of FGT? Some studies have suggested that it originates from the Stoner instability, i.e., the exchange interactions between conduction electrons lead to spontaneous spin splitting,[8,20] whereas recent studies have also discovered spectroscopic evidence for the coexistence of localized magnetic moments and conduction electrons, and their interplay is reminiscent of the Kondo-lattice physics in heavy fermion materials.[21–23] Meanwhile, many of the intriguing electronic transport properties of FGT are not well understood and remain to be explored.

In this Letter, we report temperature (T) and magnetic field (H) dependent transport studies on thin flakes of FGT, in which we observe an unusual low-temperature resistivity upturn and a nearly isotropic linear negative magnetoresistance (MR). The resistiv-

*Corresponding author. Email: yang.xu@iphy.ac.cn
© 2022 Chinese Physical Society and IOP Publishing Ltd

ity upturn obeys a $-\ln T$ to a $-T^{1/2}$ (non-Fermi liquid) crossover as well as a lower-temperature deviation (characterized by a temperature T_d). We find that it cannot be attributed to the magnetic Kondo impurity scatterings nor other mechanisms such as weak localization or electron-electron interactions (EEI). Upon applying an external magnetic field (parallel to the sample normal) up to 9 T, the upturn behavior is slightly suppressed. The FGT has a strong out-of-plane magnetic anisotropy. In the field-tilt magneto-transport measurements, we discover that the resistivity always displays a negative and linear dependence on H whenever the magnetization $\boldsymbol{M}$ is forced into the direction of $\boldsymbol{H}$. The magnitude of the MR slope is strongly enhanced at low temperatures ($\sim -T^{1/2}$), in direct contrast to the linear MR due to magnon scatterings typically found in ferromagnets. An orbital two-channel Kondo (2CK) effect and a Zeeman effect contribution are proposed to explain the anomalous transport behaviors.

Experimental Details. The layered FGT shows a spontaneous magnetization with an easy axis perpendicular to the Fe_3Ge slabs and parallel to the c axis below its Curie temperature T_c. The x-ray diffraction pattern indicates that it has a hexagonal crystal structure with the space group $P6_3/mmc$, which contains two inequivalent Fe sites Fe I and Fe II.[16,24] As shown in the side view of the lattice structure [Fig. 1(a)], FGT consists of a layer of planar FeGe (with iron atoms labeled as Fe II) sandwiched between two layers of buckling FeTe (with iron atoms labeled as Fe I). The Curie temperature T_c can be lowered to ∼150 K if substantial amount of Fe II vacancies is introduced.[11,15,16]

Single crystals of FGT were grown by the self-flux method. The high purity starting materials of Fe, Ge, and Te were mixed in an Ar-filled glove box at a molar ratio of Fe : Ge : Te = 19 : 3 : 28. The mixture was loaded into an alumina crucible and then sealed in an evacuated quartz tube. The tube was heated up to 1150 ℃ over 10 h and held for 24 h. After that, the tube was slowly cooled to 750 ℃ with a rate of 2 ℃/h. Then the centrifugation was used to separate the crystal from the flux at 750 ℃. Shiny plate-like crystals with typical dimensions of $10 \times 20 \times 1\,\mathrm{mm}^3$ were obtained.

We adopted the Scotch tape method and exfoliated the isolated thin hBN and FGT layers onto silicon or polydimethylsiloxane (PDMS) substrates.[25] The thickness of the FGT layers was measured by an atomic force microscope (typically to be 15–90 nm, yielding similar transport behaviors). The Hall-bar Pd/Au (2/15 nm) metal electrodes were pre-patterned on silicon (with 300-nm-thick SiO_2 coating) substrates by standard UV or e-beam lithography and e-beam evaporation. The dry transfer method was used to pick up hBN flakes (∼20 nm) and subsequently FGT flakes using poly-propylene carbonate (PPC) stamps.[26] Finally, the hBN/FGT heterostructure was released onto the pre-patterned electrodes and the PPC was dissolved in chloroform. All the fabrication processes (exfoliation and assembly) were carried out inside an inert gas glovebox with oxygen and water levels maintained well below 1 ppm. Here, the hBN flakes are used to protect the FGT flake from degradation. However, we note that even in samples without hBN encapsulation, they exhibit consistent transport behaviors.

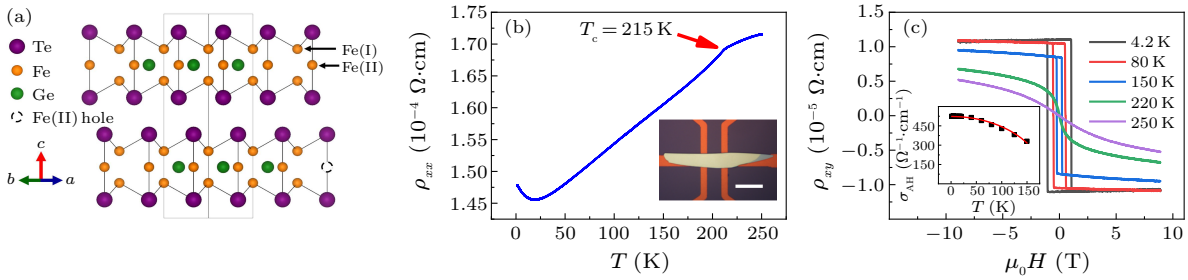

Fig. 1. (a) Crystal structure of FGT. (b) Temperature dependence of longitudinal resistivity ρ_{xx} of a representative FGT sample (83-nm-thick device A, with its optical image showing in the inset). The scale bar is 20 μm. At the Curie temperature T_c (denoted by the arrow), $d\rho_{xx}/dT$ has a discontinuity. (c) Hall resistivity ρ_{xy} as a function of magnetic field (out-of-plane) at selected temperatures from 4.2 to 250 K. The inset is the anomalous Hall conductivity σ_{xy}^{A} (solid squares) and its fit (red curve) as a function of temperature.

For transport measurements, the device was loaded into ^{4}He cryostat, with a temperature variable between 1.6 and 250 K and a magnetic field up to 9 T, or in a ^{3}He cryostat with the base temperature down to 300 mK and magnetic field up to 9 T. We have checked ohmic contacts of our samples. Four-terminal longitudinal resistance and Hall resistance were measured using standard low frequency lock-in techniques with an excitation current of 1 μA. Our measurements have been carried out on several FGT flakes exfoliated from bulk FGT. All the data shown in the main text were taken from two FGT devices measured in the ^{4}He or ^{3}He cryostat.

Figure 1(b) shows the temperature dependence (down to 1.6 K) of the longitudinal resistivity ρ_{xx} of a representative 83-nm-thick FGT Hall bar de-

vice A (optical micrograph in lower-right inset). The high-temperature kink in $\rho_{xx}(T)$ corresponds to the ferromagnetic phase transition with $T_c \sim 215\,\mathrm{K}$, which is close to the value measured in bulk crystals.[11,15,16] The low-temperature resistivity exhibits a non-monotonic behavior with a minimum appearing at $T_m \sim 20\,\mathrm{K}$, below which the increase of resistivity does not show any hint of saturation down to 1.6 K. This upturn behavior of FGT clearly deviates from the characteristic of a Fermi liquid and has been noticed in comparison with the previous studies,[8,10,12,27] but the origin is so far not well understood.[12,27] Meanwhile, the Hall resistivity ρ_{xy} develops nearly rectangular hysteresis loops with sharp jumps at low temperatures when applying a perpendicular external magnetic field $\mu_0 H$ [Fig. 1(c)]. The coercive field reaches ∼1.1 T at 4.2 K. The remanent ρ_{xy} and coercive field vanishes at around 220 K, consistent with the T_c extracted from the kink feature of ρ_{xx} in Fig. 1(b). The anomalous Hall effect (AHE) on crystalline FGT nanoflakes with different thicknesses (even down to monolayer) has been reported.[10,28] It has been suggested that the AHE is dominated by the intrinsic KL mechanism owing to the large Berry curvature from the nodal lines in the electronic band structure.[11–13] For itinerant ferromagnet, the spontaneous magnetization M is proportional to $\sqrt{1-(T/T_c)^2}$ according to the Edwards–Wohlfarth theory.[29] We notice that the anomalous Hall conductivity σ_{xy}^{A} (calculated from the magnitude of $\rho_{xy}/(\rho_{xx}^2+\rho_{xy}^2)$ at zero field) of FGT also follows a $\sqrt{1-(T/T_c)^2}$ dependence below ∼150 K [inset of Fig. 1(c)].

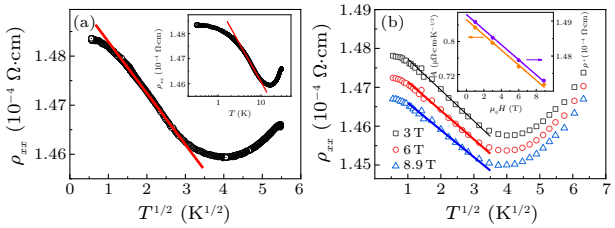

Fig. 2. (a) The longitudinal resistivity ρ_{xx} versus $T^{1/2}$ at 0 T of device B. The inset shows the same data with the temperature plotted in a logarithmic scale. The solid lines are of guides to the eyes. (b) The temperature dependences of ρ_{xx} at a few different magnetic fields, with all the data extracted from the MR measurements at different temperatures. The corresponding color-coded lines are linear fits, indicating the $T^{1/2}$ dependences. The inset shows the extracted parameters A and ρ^* as functions of the magnetic field and the linear dependences (solid lines).

To gain more insights on the resistivity upturn at low temperatures, we have conducted measurements on another 86-nm-thick device B down to 0.3 K (Fig. 2). In this sample, the minimum of $\rho_{xx}(T)$ is observed at $T_m \sim 16\,\mathrm{K}$. We plot the $\rho_{xx}(T)$ in a $T^{1/2}$ scale [Fig. 2(a)] and a logarithmic scale [inset of Fig. 2(a)], respectively. As can be seen, the $\rho_{xx}(T)$ exhibits a crossover from a marginal $-\ln T$ dependence to a $-T^{1/2}$ dependence (guided by the red solid lines) for the upturn behavior. The ρ_{xx} shows slight saturation behavior below a deviation (from the $-T^{1/2}$ dependence) temperature $T_d \sim 1.8\,\mathrm{K}$. In Fig. 2(b), we plot the $\rho_{xx}(T)$ under a few different magnetic fields applied perpendicular to the sample. The upturn behavior for T below the resistivity minimum temperature T_m maintains up to a large magnetic field of $\mu_0 H \sim 9\,\mathrm{T}$. The corresponding color-coded lines are linear fits with $\rho_{xx} = -AT^{1/2} + \rho^*$ for the low-temperature $T^{1/2}$ dependences, with the corresponding fitting parameters A and ρ^* shown in the inset of Fig. 2(b). Both A and ρ^* show weakly linear suppression upon applying the magnetic field, with slope $\alpha = -0.0183\,\mu\Omega\cdot\mathrm{cm}\cdot\mathrm{K}^{-1/2}\cdot\mathrm{T}^{-1}$ and $\beta = -0.215\,\mu\Omega\cdot\mathrm{cm}\cdot\mathrm{T}^{-1}$, respectively.

A few mechanisms are known to give rise to resistivity enhancements at low temperatures, i.e., weak localization,[30,31] enhanced EEI,[31] the spin Kondo effect[32] (due to scattering by magnetic impurities), and orbital Kondo effect[33] (scattering by structural two-level systems, non-magnetic origin). Although in three-dimensional disordered systems, the presence of EEI and localization can give rise to a $-T^{1/2}$ scaling,[31] we note that they are unlikely to account for the observations in FGT. First, weak localization can hardly happen in strong magnets with long-range magnetic order. It also contradicts the observation of non-saturating linear negative MR that we would introduce later. Meanwhile, the deviation from the $-T^{1/2}$ behavior below ∼1.8 K can hardly be explained by the EEI since the interaction contribution term typically holds well down to tens of mK.[34,35]

The presence of spin Kondo effect can also be ruled out for similar reasons. Any exchange fields between local moments or external magnetic field can lead to a strong reduction of the Kondo scattering. The canonical one-channel (no channel degeneracy) Kondo-type behavior, a crossover from a $-\ln T$ dependence (due to spin-flip scatterings of itinerant electrons off localized magnetic impurities) to a Fermi-liquid $-T^2$ dependence (due to fully screened magnetic moments at lower temperatures), is not directly observed here.[36] In more general scenarios, the spin $S = 1/2$ magnetic impurity can couple to N (>1) conduction-electron channels or Fermi reservoirs, leading to the multichannel Kondo problem. In contrast to the above one-channel ($N = 2S = 1$) case where perfect screening emerges for $T \to 0$, the impurity spin will be over-screened at $N > 2S$. For the special $N = 2$ case (referred to as the two-channel Kondo or 2CK effect), a non-Fermi liquid behavior with the scattering rate following a $-T^{1/2}$ law is predicted in the overcompensated regime. However, the experimen-

tal realization remains difficult owing to the strict requirement for zero local magnetic field and channel symmetry.[37] Meanwhile, this resistivity upturn seems to be insensitive to the concentration of Fe vacancies as similar upturn behavior is observed in Fe-deficient $Fe_{2.64}Ge_{0.87}Te_2$.[12] The local Fe vacancies that can provide Kondo holes would not account for the Kondo scatterings.[38] The resistivity upturn also emerges well below the incoherent-to-coherent crossover temperature ($T^* \sim 110$ K found for the Kondo lattice behavior) where any local moments should already be completely screened by the itinerant electrons.[21]

An analogue to the spin Kondo effect is the so-called orbital Kondo effect. As shown by Zawadowski *et al.*,[33,37] resonant tunneling two level systems (where a tunneling entity coherently tunnels between two independent quantum wells) can act as dynamical structural defects and interact with the conduction electrons through the 2CK model. Such dynamical structural defects play the role of pseudospin-1/2 scattering centers and the channel index of 2 arises from the silent spin degeneracy of the conduction electrons. Theoretical calculations have suggested three temperature regimes for distinct resistivity (or scattering time) behaviors of such orbital 2CK effects: (1) $-\ln T$ dependence above the Kondo temperature T_K; (2) $-T^{1/2}$ dependence for $T_d < T \ll T_K$, where $T_d = \Delta^2/T_K$ and Δ is the effective energy splitting of the two levels; (3) lower temperature deviation from the $-T^{1/2}$ dependence at $T < T_d$.[37,39] Compared to the spin 2CK effect, the orbital 2CK effect can be realized in less stringent conditions.[33,40] Experimental evidence for the orbital 2CK effects has been reported for both nonmagnetic and magnetic systems (e.g., ThAsSe and $L1_0$-MnAl films).[41–45] Similar to the identification of the three temperature regimes first demonstrated in the $L1_0$-MnAl films,[44] the crossover from $-\ln T$ to $-T^{1/2}$ dependences and the lower-temperature saturation could suggest FGT another platform for investigating this intriguing orbital 2CK effect. A deviation from the $-\ln T$ behavior is identified at ~4.7 K [inset of Fig. 2(a)], which we assign to be the Kondo temperature T_K.[44] We note that this substantially smaller orbital T_K is not relevant to the previous studies showing the spin Kondo temperature ~190 K for the Kondo lattice behavior in the Fe-deficient FGT.[21] The temperature scale that sets the lower bound for the $-T^{1/2}$ dependence is Δ^2/T_K (estimated to be $T_d \approx 1.8$ K),[46] through which we can extract the effective energy splitting of the two levels to be $\Delta \approx 2.9$ K.

We notice that the H dependence of A is negligible in ThAsSe and $L1_0$-MnAl,[42,44] while in FGT the A coefficient is linearly suppressed by H. It is likely related to the larger channel asymmetry (due to imbalance between spin-up and spin-down charge carriers in the conduction band) of FGT with strong magnetization. The tunability is consistent with the expectation that a magnetic field can quench the 2CK scatterings at a rate proportional to H.[41,46] The argument is further supported by our detailed MR studies discussed below.

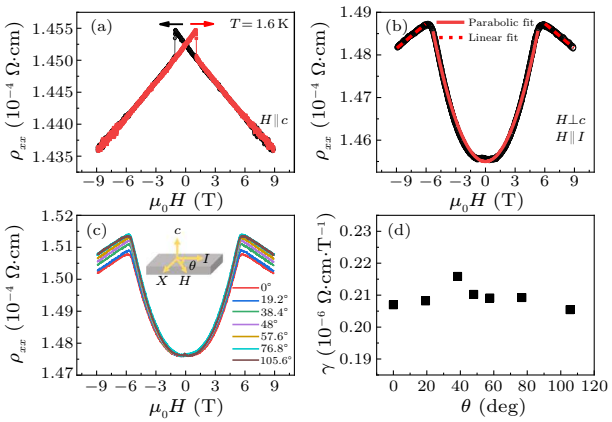

Fig. 3. The magnetic field dependence of longitudinal resistivity (device A) at 1.6 K in the field direction $\boldsymbol{H}$ parallel (a) and perpendicular [(b), (c)] to the film normal. The arrows shown in (a) represent sweeping up/down the magnetic field. The solid and dashed curves shown in (b) are the corresponding fits to H^2 and H dependences before and after $\mu_0 H$ reaches the anisotropy field $H_A \sim \pm 5.7$ T, respectively. In the parallel field configuration, θ denotes the angle between $\boldsymbol{H}$ and I. (d) The extracted slope magnitude γ from the H linear regions ($>\mu_0 H_A \sim 5.7$ T) plotted as a function of θ, indicating the linear negative MR barely has any dependence on the orientation of the in-plane field.

Figures 3(a)–3(c) present the out-of-plane (with $\boldsymbol{H}$ being parallel to the film normal c axis) and in-plane ($\boldsymbol{H}$ perpendicular to the c axis, with varying the angle θ between $\boldsymbol{H}$ and the current I) magnetic field dependences of ρ_{xx} at $T = 1.6$ K. In the out-of-plane field configuration [Fig. 3(a)], a bow-tie shaped hysteresis loop is observed with field sweeping up and down. Sharp jumps in ρ_{xx} occur at the coercive field $\mu_0 H = \pm 1.1$ T, concomitant with the magnetization (M) reversal process. Another prominent feature is the linear and non-saturating negative MR (with slope magnitude $\gamma = |\frac{d\rho_{xx}}{d(\mu_0 H)}| = 0.179\ \mu\Omega \cdot \text{cm} \cdot \text{T}^{-1}$), which persists up to the largest field (9 T) applied. The sharp magnetic switches in the AHE [Fig. 1(c)] and MR indicate a single magnetic domain over the entire flake at low temperatures. It rules out the negative MR typically found in soft ferromagnets due to domain wall motions. As shown in Figs. 3(b) and 3(c), when the magnetic field is applied parallel to the sample plane and perpendicular to the magnetic antitropy easy axis (c axis), no magnetic hysteresis is observed as expected. The MR shows positive and quadratic dependence on H before it reaches a turning point at which the MR becomes linear negative again. The quadratic MR at $\boldsymbol{H} \perp c$ can be satisfactorily explained by the anisotropic magnetoresistance (AMR)

effect commonly seen in ferromagnets.[47] The magnetization canting angle φ induced by the in-plane field H has the form $\sin\varphi = \chi_{ab}H/M_s$, where χ_{ab} is the magnetic susceptibility in the ab plane and M_s is the saturated magnetization. When the scattering rate is higher for electrons moving parallel to $\boldsymbol{M}$ compared to being perpendicular, the in-plane field can drive a resistance enhancement proportional to $(\chi_{ab}H/M_s)^2$. Similar effect has also been reported for layered ferromagnet $Fe_{1/4}TaS_2$.[48] The turning point at $\sim\pm5.7$ T is identified as the anisotropy field $\mu_0 H_A$, beyond which the magnetization M is fully saturated to the $\boldsymbol{H}$ direction and the AMR effect no longer contributes to the MR. The $\mu_0 H_A$ value observed in our thin flakes is also consistent with previous magnetization measurements on bulk crystals.[23] For $H > H_A$, the slope of the linear negative MR has the magnitude slightly larger than that measured in the out-of-plane configuration ($\sim$15% difference). We have also checked that the slope magnitude γ barely has any dependence on the angle between the in-plane $\boldsymbol{H}$ and current I [see Fig. 3(d)].

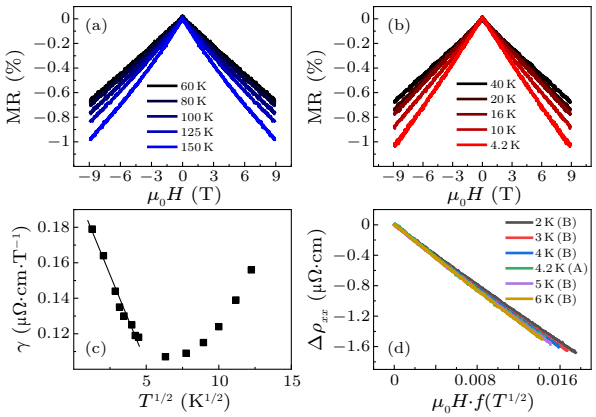

Fig. 4. [(a), (b)] MR curves at selected temperatures (device A), in which only the sweeps from high magnetic fields toward zero field are included. (c) The extracted slope magnitude γ of MR curves as a function of temperature. The solid line is a $T^{1/2}$ dependence fit at low temperatures. (d) $\Delta\rho_{xx}$ vs $\mu_0 H \cdot f(T^{1/2})$, where $f(T^{1/2})$ is the linear function of $T^{1/2}$. Here A and B represents devices A and B, respectively.

In Fig. 4, we present the MR study in the out-of-plane field configuration at different temperatures. For clarity, only the data for magnetic field swept from high to zero are shown. The data do not involve the process across the coercive fields and hence no hysteresis is expected. Here the non-saturating linear negative MR is observed up to temperatures as high as $\sim$150 K [Fig. 4(a)]. The slope $\gamma = |d\rho_{xx}/d\mu_0 H|$ shows a nonmonotonic temperature dependence [Fig. 4(c)]. Above $\sim$40 K, its magnitude gets enhanced with increasing temperature, whereas below 40 K the trend is opposite [Fig. 4(b)]. The γ value increases by $\sim$70% from 40 K to the base temperature and nearly follows a $-T^{1/2}$ dependence. In ferromagnets, the magnon population can be linearly suppressed by external magnetic fields, which reduces the magnon/spin scattering to the charge carriers.[48–51] Though this mechanism could contribute to the negative MR with H linear dependences at high temperatures in FGT, it can hardly explain the low-T enhancement of γ as the magnon population is exponentially suppressed upon cooling down.[49] We also notice that the linear MR has been proposed as a consequence of magnetic-field-induced modification to the phase-space volume owing to the nonzero Berry curvature ($\boldsymbol{\Omega}$) in the momentum space, with the leading order proportional to $\boldsymbol{H} \cdot \boldsymbol{\Omega}$.[52,53] However, considering the strongly anisotropic band structure and Berry curvatures of FGT, it should give rise to substantially different responses when changing the direction of $\boldsymbol{H}$ from out-of-plane to in-plane. The nearly isotropic linear MR observed in our experiments indicates negligible contributions from this intrinsic Berry curvature effect.

We now consider the two-band Drude model incorporating the spin-up and spin-down charge carriers separately for a ferromagnet. The conductivity can then be expressed as

$$\sum_{\sigma}\frac{e^2 n_\sigma \tau_\sigma}{m^*} = \frac{e^2}{2m^*}[(n_\uparrow - n_\downarrow)(\tau_\uparrow - \tau_\downarrow) + (n_\uparrow + n_\downarrow)(\tau_\uparrow + \tau_\downarrow)],$$

where σ ($\uparrow$ or $\downarrow$) denotes the spin index and m^* is the effective mass, $n_\uparrow$ and $n_\downarrow$ are the densities of majority (up) and minority (up) spins in the system. The electrons with spin parallel ($\uparrow$) and antiparallel ($\downarrow$) to $\boldsymbol{M}$ have different scattering times $\tau_\uparrow$ and $\tau_\downarrow$.[54] The carrier densities $n_\uparrow$ and $n_\downarrow$ are tuned linearly by H (when $\boldsymbol{H}//\boldsymbol{M}$) through the Zeeman energy shift at the Fermi surface, while keeping the total density $n = n_\uparrow + n_\downarrow$ conserved. To the first order approximation, the field induced correction to the MR is then proportional to $\Delta n = (n_\uparrow - n_\downarrow) \sim \mu_0 H$.[55,56] While this mechanism can give rise to a finite linear MR at the base temperature, it cannot explain the lower-temperature enhancement of γ since at $T \ll T_C$ both the scattering time and Δn should be saturated.

In Fig. 4(d), we plot $\Delta\rho_{xx}$ vs $\mu_0 H \cdot f(T^{1/2})$ for the scaled MR curves taken in two different samples (A and B) between 2–6 K (within the $-T^{1/2}$ dependence region), where $\Delta\rho_{xx} = \rho_{xx}(H) - \rho_{xx}(H=0)$ and $f(T^{1/2}) = -\alpha T^{1/2} + \beta$ is linear function of $T^{1/2}$, with the parameter α and β determined earlier. The data measured at different temperatures nearly collapse onto the same curve, revealing a scaling behavior. It indicates the contribution to resistivity change at low temperatures depends on $-\alpha H T^{1/2}$ and a temperature-independent part βH. The first term could stem from the field suppression of the orbital 2CK effect with a scaling function $\propto HT^{1/2}$. The second term is temperature-independent and possibly attribute to the Zeeman shift effect at the Fermi sur-

face discussed above.

In summary, we discover anomalous transport phenomena in FGT thin flakes and provide possible explanations. The most intriguing finding is the non-saturating negative linear MR over a broad temperature range and the non-monotonic temperature dependence of the MR slope γ. We attribute the higher-temperature linear MR mainly to the field-induced suppression of magnon scatterings. This mechanism would suppress the slope γ monotonically with decreasing temperature. The 2CK effect offers a possible explanation of the lower-temperature upturn of the slope γ, which follows a $-T^{1/2}$ dependence. In such a scenario, the crossover temperature $\sim$40 K is a measure of the related energy scales. It would be of great interest for future studies to keep looking for microscopic evidence (such as those from scanning tunneling microscopy) for the existence of structural two-level impurities (tunneling centers) to support the proposed orbital 2CK effect in the ferromagnetic FGT. Such multichannel Kondo effect is of great interest to the community due to its relevance of exotic and non-Fermi-liquid properties that can be found in various quantum material systems such as strong correlated materials, metallic glasses, quantum dots, and topological qubits.[37,41–43,57–59] Our work would be helpful for understanding the anomalous transport behaviors and rich interaction phenomena in such systems.

Acknowledgments. This work was supported by the National Natural Science Foundation of China (Grant Nos. 12174439, 11961141011, U2032204, and 12074039), and the Strategic Priority Research Program of Chinese Academy of Sciences (Grant Nos. XDB28000000 and XDB33030000).

References

[1] Gong C and Zhang X 2019 *Science* **363** eaav4450
[2] Mak K F, Shan J and Ralph D C 2019 *Nat. Rev. Phys.* **1** 646
[3] Gibertini M, Koperski M, Morpurgo A F and Novoselov K S 2019 *Nat. Nanotechnol.* **14** 408
[4] Fisher M E 1974 *Rev. Mod. Phys.* **46** 597
[5] Jiang S, Li L, Wang Z, Mak K F and Shan J 2018 *Nat. Nanotechnol.* **13** 549
[6] Jiang S, Shan J and Mak K F 2018 *Nat. Mater.* **17** 406
[7] Huang B, Clark G, Klein D R, MacNeill D, Navarro-Moratalla E, Seyler K L, Wilson N, McGuire M A, Cobden D H, Xiao D, Yao W, Jarillo-Herrero P and Xu X 2018 *Nat. Nanotechnol.* **13** 544
[8] Deng Y, Yu Y, Song Y, Zhang J, Wang N Z, Sun Z, Yi Y, Wu Y Z, Wu S, Zhu J, Wang J, Chen X H and Zhang Y 2018 *Nature* **563** 94
[9] Wang Z, Zhang T, Ding M, Dong B, Li Y, Chen M, Li X, Huang J, Wang H, Zhao X, Li Y, Li D, Jia C, Sun L, Guo H, Ye Y, Sun D, Chen Y, Yang T, Zhang J, Ono S, Han Z and Zhang Z 2018 *Nat. Nanotechnol.* **13** 554
[10] Fei Z, Huang B, Malinowski P, Wang W, Song T, Sanchez J, Yao W, Xiao D, Zhu X, May A F, Wu W, Cobden D H, Chu J H and Xu X 2018 *Nat. Mater.* **17** 778
[11] Kim K, Seo J, Lee E, Ko K T, Kim B S, Jang B G, Ok J M, Lee J, Jo Y J, Kang W, Shim J H, Kim C, Yeom H W, Il Min B, Yang B J and Kim J S 2018 *Nat. Mater.* **17** 794
[12] Liu Y, Stavitski E, Attenkofer K and Petrovic C 2018 *Phys. Rev. B* **97** 165415
[13] Wang Y, Xian C, Wang J, Liu B, Ling L, Zhang L, Cao L, Qu Z and Xiong Y 2017 *Phys. Rev. B* **96** 134428
[14] Lin X and Ni J 2019 *Phys. Rev. B* **100** 085403
[15] Deiseroth H J, Aleksandrov K and Reiner C 2006 *Eur. J. Inorg. Chem.* **2006** 1561
[16] May A F, Calder S, Cantoni C, Cao H and McGuire M A 2016 *Phys. Rev. B* **93** 014411
[17] Wang Z, Sapkota D, Taniguchi T, Watanabe K, Mandrus D and Morpurgo A F 2018 *Nano Lett.* **18** 4303
[18] Zhu W, Lin H, Yan F, Hu C, Wang Z, Zhao L, Deng Y, Kudrynskyi Z R, Zhou T, Kovalyuk Z D, Zheng Y, Patanè A, Žutić I, Li S, Zheng H and Wang K 2021 *Adv. Mater.* **33** 2104658
[19] Hu C, Zhang D, Yan F, Li Y, Lv Q, Zhu W, Wei Z, Chang K and Wang K 2020 *Sci. Bull.* **65** 1072
[20] Zhuang H L, Kent P R C and Hennig R G 2016 *Phys. Rev. B* **93** 134407
[21] Zhang Y, Lu H Y, Zhu X G, Tan S Y, Feng W, Liu Q, Zhang W, Chen Q Y, Liu Y, Luo X B, Xie D H, Luo L Z, Zhang Z J and Lai X C 2018 *Sci. Adv.* **4** eaao6791
[22] Xu X, Li Y W, Duan S R, Zhang S L, Chen Y J, Kang L, Liang A J, Chen C, Xia W, Xu Y, Malinowski P, Xu X D, Chu J H, Li G, Guo Y F, Liu Z K, Yang L X and Chen Y L 2020 *Phys. Rev. B* **101** 201104
[23] Bao S, Wang W, Shangguan Y, Cai Z, Dong Z Y, Huang Z, Si W, Ma Z, Kajimoto R, Ikeuchi K, Yano S I, Yu S L, Wan X, Li J X and Wen J 2022 *Phys. Rev. X* **12** 011022
[24] Zhu J X, Janoschek M, Chaves D S, Cezar J C, Durakiewicz T, Ronning F, Sassa Y, Mansson M, Scott B L, Wakeham N, Bauer E D and Thompson J D 2016 *Phys. Rev. B* **93** 144404
[25] Novoselov K S, Geim A K, Morozov S V, Jiang D, Zhang Y, Dubonos S V, Grigorieva I V and Firsov A A 2004 *Science* **306** 666
[26] Wang L, Meric I, Huang P Y, Gao Q, Gao Y, Tran H, Taniguchi T, Watanabe K, Campos L M, Muller D A, Guo J, Kim P, Hone J, Shepard K L and Dean C R 2013 *Science* **342** 614
[27] Verchenko V Y, Tsirlin A A, Sobolev A V, Presniakov I A and Shevelkov A V 2015 *Inorg. Chem.* **54** 8598
[28] Tan C, Lee J, Jung S G, Park T, Albarakati S, Partridge J, Field M R, McCulloch D G, Wang L and Lee C 2018 *Nat. Commun.* **9** 1554
[29] Edwards D M, Wohlfarth E P and Jones H 1968 *Proc. R. Soc. London A* **303** 127
[30] Bergmann G 1984 *Phys. Rep.* **107** 1
[31] Lee P A and Ramakrishnan T V 1985 *Rev. Mod. Phys.* **57** 287
[32] Kondo J 1964 *Prog. Theor. Phys.* **32** 37
[33] Zawadowski A 1980 *Phys. Rev. Lett.* **45** 211
[34] Rapp Ö, Bhagat S M and Gudmundsson H 1982 *Solid State Commun.* **42** 741
[35] Yang S, Li Z, Lin C, Yi C, Shi Y, Culcer D and Li Y 2019 *Phys. Rev. Lett.* **123** 096601
[36] Hewson A C 1993 *The Kondo Problem to Heavy Fermions* (Cambridge: Cambridge University Press)
[37] Cox D L and Zawadowski A 1998 *Adv. Phys.* **47** 599
[38] Zhao M, Chen B B, Xi Y, Zhao Y, Xu H, Zhang H, Cheng N, Feng H, Zhuang J, Pan F, Xu X, Hao W, Li W, Zhou S, Dou S X and Du Y 2021 *Nano Lett.* **21** 6117
[39] von Delft J, Ralph D C, Buhrman R A, Upadhyay S K, Louie R N, Ludwig A W W and Ambegaokar V 1998 *Ann. Phys.* **263** 1
[40] Zaránd G 2005 *Phys. Rev. B* **72** 245103
[41] Ralph D C, Ludwig A W W, von Delft J and Buhrman R A 1994 *Phys. Rev. Lett.* **72** 1064
[42] Cichorek T, Sanchez A, Gegenwart P, Weickert F, Wojakowski A, Henkie Z, Auffermann G, Paschen S, Kniep R and Steglich F 2005 *Phys. Rev. Lett.* **94** 236603

[43] Kirchner S 2020 *Adv. Quantum Technol.* **3** 1900128
[44] Zhu L J, Nie S H, Xiong P, Schlottmann P and Zhao J H 2016 *Nat. Commun.* **7** 10817
[45] Cichorek T, Bochenek L, Schmidt M, Czulucki A, Auffermann G, Kniep R, Niewa R, Steglich F, and Kirchner S 2016 *Phys. Rev. Lett.* **117** 106601
[46] Affleck I, Ludwig A W W, Pang H B and Cox D L 1992 *Phys. Rev. B* **45** 7918
[47] McGuire T and Potter R 1975 *IEEE Trans. Mag.* **11** 1018
[48] Checkelsky J G, Lee M, Morosan E, Cava R J and Ong N P 2008 *Phys. Rev. B* **77** 014433
[49] Gil W, Görlitz D, Horisberger M and Kötzler J 2005 *Phys. Rev. B* **72** 134401
[50] Raquet B, Viret M, Sondergard E, Cespedes O and Mamy R 2002 *Phys. Rev. B* **66** 024433
[51] Boye S A, Lazor P and Ahuja R 2005 *J. Appl. Phys.* **97** 083902
[52] Xiao D, Shi J and Niu Q 2005 *Phys. Rev. Lett.* **95** 137204
[53] Xiao D, Chang M C and Niu Q 2010 *Rev. Mod. Phys.* **82** 1959
[54] Kasuya T 1956 *Prog. Theor. Phys.* **16** 58
[55] Wang Y, Lee P A, Silevitch D M, Gomez F, Cooper S E, Ren Y, Yan J Q, Mandrus D, Rosenbaum T F and Feng Y 2020 *Nat. Commun.* **11** 216
[56] Smit J 1951 *Physica* **17** 612
[57] Potok R M, Rau I G, Shtrikman H, Oreg Y and Goldhaber-Gordon D 2007 *Nature* **446** 167
[58] Yeh S S and Lin J J 2009 *Phys. Rev. B* **79** 012411
[59] Béri B and Cooper N R 2012 *Phys. Rev. Lett.* **109** 156803